

# Bayesian Indicator-Saturated Regression for Climate Policy Evaluation

LUCAS D. KONRAD<sup>†</sup>, LUKAS VASHOLD<sup>‡</sup> AND JESUS CRESPO CUARESMA<sup>\*</sup>

<sup>†</sup> *WU Vienna University of Economics and Business,  
Welthandelsplatz 1, 1020 Vienna (Austria)*  
E-mail: [lucas.konrad@wu.ac.at](mailto:lucas.konrad@wu.ac.at)

<sup>‡</sup> *WU Vienna University of Economics and Business*

<sup>\*</sup> *WU Vienna University of Economics and Business,  
Wittgenstein Centre for Demography and Global Human Capital,  
Austrian Institute of Economic Research*

## Summary

Structural break identification methods are an important tool for evaluating the effectiveness of climate change mitigation policies. In this paper, we introduce a unified probabilistic framework for detecting structural breaks with unknown timing and arbitrary sequence in longitudinal data. The proposed Bayesian setup uses indicator-saturated regression and a spike-and-slab prior with an inverse-moment density as the slab component to ensure model selection consistency. Simulation results show that the method outperforms comparable frequentist approaches, particularly in environments with a high probability of structural breaks. We apply the framework to identify and evaluate the effects of climate policies in the European road transport sector.

**Keywords:** *Structural breaks, climate policy evaluation, model selection, spike-and-slab priors, indicator saturation*

## 1. INTRODUCTION

Recent contributions to the empirical identification of climate change mitigation policies exploit systematic variation in carbon emissions data to detect structural changes associated with policy interventions (Koch et al., 2022; Stechemesser et al., 2024; Tebecis and Crespo Cuaresma, 2025). Within this framework, policy effects are operationalized as statistically significant level shifts identified using indicator-saturated regression (ISR) methods (Castle et al., 2015; Pretis and Schwarz, 2022). ISR provides a general-to-specific modelling strategy that enables the detection of multiple structural breaks without prior knowledge of their timing.

In conventional program evaluation settings, ex post analyses are based on interventions with known implementation dates that affect a subset of units (the treated group), with inference based on comparisons to unaffected units (the control group). Under the assumption of conditional ignorability of treatment assignment, this framework delivers consistent estimates of causal treatment effects (see, for example, Imbens and Wooldridge, 2009). Climate change mitigation policies, however, are typically enacted at the national or supranational level and target multiple emissions-generating sectors simultaneously. Moreover, they are rarely implemented in isolation and frequently interact with other regulatory and fiscal instruments. This institutional environment limits the availability of quasi-experimental variation in policy exposure and thereby complicates the application of conventional causal inference methods based on cross-sectional or temporal contrasts.

Given these identification challenges, the empirical literature has increasingly relied on structural break detection in emissions time series as an indirect strategy for identifying

policy effects. Detected breaks are subsequently attributed to specific policy interventions or bundles of measures using institutional and historical information. This approach has been applied to global climate policy assessments (Stechemesser et al., 2024), to sector-specific analyses such as EU transport (Koch et al., 2022), to subnational evidence from Canadian provinces (Pretis, 2022), and to the construction of harmonized datasets of emission breakpoints (Tebecis and Crespo Cuaresma, 2025).

In this paper, we develop a Bayesian extension of the ISR framework tailored to high-dimensional structural break detection in macro-environmental panel data. While existing contributions rely on frequentist selection procedures within ISR (Castle et al., 2015; Pretis and Schwarz, 2022), we embed break detection in a fully probabilistic model selection framework. As in Pretis and Schwarz (2022) and Stechemesser et al. (2024), our approach considers an unknown number of structural breaks of unknown timing, but departs from these contributions by introducing a flexible Bayesian setup with a spike-and-slab prior that combines a Dirac spike and a non-local slab component. This prior structure yields model selection consistency in the ISR framework, penalises weak signals more aggressively than conventional local priors, and delivers coherent posterior uncertainty quantification in a unified framework. Our particular choice of non-local prior, the inverse moment (iMOM) prior (see Johnson and Rossell, 2010), exhibits Cauchy-like tails, thus imposing minimal shrinkage on large signals in line with Jeffreys (1998) and Bayarri and García-Donato (2007). In addition, the model explicitly accommodates the presence of outlying observations, improving robustness in applications with noisy data while remaining computationally tractable in high-dimensional settings.

We evaluate the finite-sample performance of the proposed estimator in a comprehensive simulation study and benchmark it against leading frequentist procedures for structural break detection. The results indicate that our approach performs comparably well in sparse designs and exhibits clear advantages in environments characterised by multiple or closely spaced breaks.

Applying the method to European road transport emissions, we replicate the main findings of (Koch et al., 2022) while uncovering systematic differences in policy attribution. In particular, our attribution analysis suggests that a broader set of policy interventions than previously identified contributed to the observed reductions in transport emissions.

The remainder of the paper is organised as follows. Section 2 presents the proposed framework, which we term Bayesian Indicator Saturated Modelling (BISAM). Section 3 evaluates its finite-sample performance using simulated data and benchmarks it against existing frequentist approaches to structural break detection. Section 4 reports the empirical application to European road transport emissions and discusses the implications for the identification of effective climate mitigation policies. Section 5 concludes.

## 2. THE BAYESIAN INDICATOR SATURATED MODEL

In this section, we present our methodological framework for the detection of structural breaks in panel data settings. We formalise the problem of identifying an unknown number of structural breaks at unknown timing within an ISR framework, an extremely flexible model class widely used in applications to climate policy evaluation due to its interpretability (Koch et al., 2022; Stechemesser et al., 2024).

2.1. Indicator Saturated Regressions: Specification

The literature on structural break detection in time series is extensive, yet the majority of existing approaches either require long time horizons (a luxury rarely afforded by macro-environmental panel data) or impose strong restrictions on the break process. Our modelling framework uses a break function that takes the form of indicator saturation, accommodating practically every combination of transitions while performing well on relatively short time horizons.

Let  $i = 1, \dots, N$  index cross-sectional units and  $t = 1, \dots, T$  index time periods. For the observed panel  $\{(y_{i,t}, x_{i,t})\}_{i=1, \dots, N; t=1, \dots, T}$  with  $y_{i,t} \in \mathbb{R}$  and  $x_{i,t} \in \mathbb{R}^p$ , we define the *general break model*

$$y_{i,t} = f(x_{i,t}) + \sum_{s \in \mathcal{S}} \gamma_s d_s(i, t) + \varepsilon_{i,t}, \quad (2.1)$$

where  $f: \mathbb{R}^p \rightarrow \mathbb{R}$  is a mean function modelling the response under the absence of breaks.  $\mathcal{S}$  is a (potentially very large) candidate set of indicator indices, with  $q$  denoting the size of this set, i.e., the number of all possible breaks.  $\gamma_s \in \mathbb{R}$  are the associated break coefficients, and  $d_s: \{1, \dots, N\} \times \{1, \dots, T\} \rightarrow \{0, 1\}$  are indicator functions selecting the units and periods affected by break  $s$ . The disturbance term  $\varepsilon_{i,t}$  captures idiosyncratic shocks.

By choosing  $\mathcal{S}$  and the form of  $d_s$ , this formulation nests a variety of saturation approaches: impulse indicator saturation (IIS), step-shift indicator saturation (SIS), and trend indicator saturation (TIS). Following Pretis and Schwarz (2022), we concentrate on a particular specification of the model in equation (2.1), setting  $f(x_{i,t}) = x'_{i,t} \beta$  (linear mean function), indexing  $\mathcal{S}$  by pairs  $(j, s)$  with  $j \in \{1, \dots, N\}$  and  $s \in \{3, \dots, T-1\}$ ,<sup>1</sup> and defining the break function as step-shift indicators  $d_{j,s}(i, t) = \mathbb{1}_{\{i=j\}} \mathbb{1}_{\{t \geq s\}}$ . This yields the SIS linear model

$$y_{i,t} = x'_{i,t} \beta + \sum_{j=1}^N \sum_{s=3}^{T-1} \gamma_{j,s} \mathbb{1}_{\{j=i\}} \mathbb{1}_{\{t \geq s\}} + \varepsilon_{i,t}. \quad (2.2)$$

The vector  $x_{i,t}$  may include cross-sectional fixed effects, time fixed effects, and additional covariates associated with the outcome  $y_{i,t}$ . The indicator functions  $\mathbb{1}_{\{j=i\}}$  and  $\mathbb{1}_{\{t \geq s\}}$  define unit-specific step-shift indicators that take the value one for unit  $i = j$  and periods  $t \geq s$ , respectively, and zero otherwise.

In its unrestricted form, the model in equation (2.2) contains  $N(T-3) + p$  free parameters to be estimated from  $NT$  observations. This high-dimensional setting gives rise to a challenging model selection problem in practice. In a classical framework, strategies to address this curse of dimensionality include general-to-specific (GETS) block-search algorithms (Santos et al., 2008), as employed by Castle et al. (2012, 2015) and Pretis and Schwarz (2022), as well as regularisation techniques such as the (adaptive) Least Absolute Shrinkage and Selection Operator (LASSO) (Tibshirani, 1996), used by Li et al. (2016), Qian and Su (2016) and Pretis and Schwarz (2022).

We propose a fully Bayesian approach designed to address the high-dimensional model selection problem inherent in such indicator-saturated regressions. Bayesian Indicator

<sup>1</sup>Note that  $s \notin \{1, 2, T\}$  as these step-shifts are equivalent to either the unit-fixed effect or dummies capturing individual observations, and thus single-observation outliers, at the beginning or end of the sample.

Saturated Modelling (BISAM) builds on recent advances in Bayesian variable selection. The coherent probabilistic framework avoids sequential estimation and allows for efficient structural break identification as well as exact posterior uncertainty quantification.

### 2.2. Priors on the Mean Function

The prior distribution on  $\beta$ , the coefficients associated with the control variables, can be specified using standard formulations such as the independent Normal prior, Zellner's  $g$ -prior (Zellner, 1986), or the fractional ( $f$ -)prior (O'Hagan, 1995). In settings where strong variable selection of covariates is required, continuous shrinkage priors such as the horseshoe prior (Carvalho et al., 2010) can provide a flexible alternative to these settings, allowing for more aggressive shrinkage of irrelevant coefficients while preserving signals of substantive magnitude.

For the variance of the unit-specific error term, we employ an inverse gamma prior,

$$\sigma_i^2 \sim \mathcal{G}^{-1}(m_0, n_0), \quad (2.3)$$

where the hyperparameters  $m_0$  and  $n_0$  govern the prior scale and dispersion. The flexibility of the inverse gamma distribution allows for virtually uninformative setups, as well as for informative calibrations using an empirical Bayes approach. We propose benchmarking the residual variance estimates from a baseline specification that excludes structural breaks, in line with Chipman et al. (2010).

### 2.3. Priors on the Break Function

The break-size coefficients are modelled using a variant of the Stochastic Search Variable Selection (SSVS) prior. Every potential step-shift is included in the regression, and the estimation procedure enacts the selection of these. For this purpose, we consider a family of spike-and-slab mixture priors on  $\gamma_{i,s}$  (Mitchell and Beauchamp, 1988; George and McCulloch, 1993, 1997; Ishwaran and Rao, 2005). In the context of equation (2.2), this can be written as

$$p(\gamma_{i,s} | \delta_{i,s}^\gamma) = (1 - \delta_{i,s}^\gamma) p_{spike}(\gamma_{i,s}) + \delta_{i,s}^\gamma p_{slab}(\gamma_{i,s}), \quad (2.4)$$

where the binary selection indicator  $\delta_{i,s}^\gamma \in \{0, 1\}$  governs whether the coefficient  $\gamma_{i,s}$  stems from  $p_{spike}$ , a Dirac-spike concentrated at zero, or from  $p_{slab}$ , the slab density that allows for deviations from zero. Under this specification, structural break detection is naturally understood as variable selection, or equivalently, a posterior inclusion problem: a step-shift is selected whenever  $\mathbb{E}(\delta_{i,s}^\gamma | y) > P$ , for some given probability threshold  $P \in (0, 1)$ .

We impose a Bernoulli prior on the selection indicator,

$$p(\delta_{i,s}^\gamma) = \omega_{i,s}^{\delta_{i,s}^\gamma} (1 - \omega_{i,s})^{1 - \delta_{i,s}^\gamma}, \quad (2.5)$$

where  $\omega_{i,s}$  denotes the prior inclusion probability of the corresponding step-shift indicator. This parameter may be fixed ex ante or treated hierarchically and learned from the data, in line with Scott and Berger (2010).

The flexibility of the break function as given by equation (2.2) however places particular requirements on the prior design of  $\gamma_{i,s}$ . First, the prior should induce a clear separation between inclusion and exclusion in the posterior, thereby sharpening break detection while shrinking weak signals aggressively. Second, the overall prior specification should

preserve model selection consistency, which in the high-dimensional ISR framework requires consistency in a regime where the number of candidate break parameters grows linearly in  $N$  and  $T$ . Third, conditional on inclusion, the slab component should allow for flexible estimation of the break magnitude without imposing excessive shrinkage.

To satisfy these three requirements, we specify a prior with a Dirac point mass at zero for the spike component and adopt a non-local prior density for the slab component. The Dirac prior for  $p_{spike}$  sets shifts to *exactly* zero if  $\delta_{i,t} = 0$ , virtually excluding the break from estimation and thereby adding to the specificity of break detection.<sup>2</sup>

Selecting a non-local prior as slab component ensures separation from the spike by concentrating mass away from zero. Formally, a prior on the break coefficients in equation (2.2) is non-local if its density  $\pi(\gamma_{j,s})$  satisfies

$$\lim_{|\gamma_{j,s}| \rightarrow 0} \pi(\gamma_{j,s}) = 0, \quad (2.6)$$

that is, the prior density vanishes at  $\gamma_{j,s} = 0$  (see Rossell and Telesca, 2017, for details). This characteristic is crucial to meet the first two requirements described above. Under a local prior density  $\pi_L$  with  $\pi_L(0) > 0$ , the Bayes factor in favour of a spurious break decays only at rate  $\text{BF}_T(H_A | H_0 = \text{true}) = O_p(T^{-1/2})$  when the true coefficient is zero (Johnson and Rossell, 2010), implying weak penalisation of negligible breaks, particularly in panels with a short time horizon. Non-local priors accelerate this decay by assigning zero density at the origin. More importantly for model selection consistency, the indicator saturation framework implies an effective model dimension that grows as  $O(NT)$ . Johnson and Rossell (2012) show that when the number of candidate coefficients increases linearly in the number of observations, non-local priors ensure that the posterior probability of the model containing the true constellation of structural breaks converges to one as the sample size increases. Under any continuous local prior with  $\pi_L(0) > \varepsilon > 0$ , this probability instead converges to zero whenever the number of candidates exceeds  $O(T^{1/2})$  (see Theorem 2 in Johnson and Rossell, 2012).

Turning to the third requirement of the prior setting, shrinkage of genuinely large breaks is governed by the tail behaviour of the slab component. Heavy tails mitigate the bias that proper priors introduce in finite samples by reducing shrinkage of large coefficients (see Jeffreys, 1998). Among non-local prior families, the inverse-moment (iMOM) prior is particularly well suited, as it combines a vanishing density at zero with heavy tails that preserve large signals. Its density is given by

$$\pi_{iMOM}(\gamma_{i,s} | \gamma_0, k, \nu, \tau\sigma^2) = \frac{k(\tau\sigma^2)^{\nu/2}}{\Gamma(\nu/2k)} (\gamma_{i,s} - \gamma_0)^{-(\nu+1)} \exp \left\{ - \left( \frac{\gamma_{i,s} - \gamma_0}{\sqrt{\tau\sigma}} \right)^{-2k} \right\}, \quad (2.7)$$

where  $\gamma_0$  denotes the centering value,  $\nu > 0$  is a shape parameter,  $k > 0$  controls the order of the prior,  $\tau$  is a scale hyperparameter,  $\sigma^2$  is the error variance and  $\Gamma$  denotes the gamma function. The parameters  $\nu$  and  $k$  jointly determine the tail behaviour and the rate at which density vanishes near  $\gamma_0$ . In our baseline specification, we set  $\gamma_0 = 0$  and  $\nu = k = 1$ , yielding Cauchy-like tails.

<sup>2</sup>Such a choice, however, increases computational complexity when comparing marginal likelihoods across models that differ in their step-shift indicators, even when Laplace approximations are used. Alternatively, a highly concentrated Gaussian prior for the spike component can be used (see, for example, George and McCulloch, 1997; Ishwaran and Rao, 2005). Such an approach has the drawback of not fully excluding step-shift indicators, thus decreasing precision of separation for included and excluded breaks.

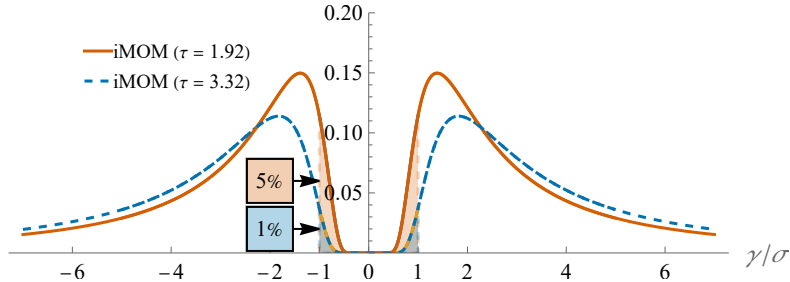


**Figure 1.** Probability density function of  $iMOM(0, 1, 1, \tau)$  prior for the cases  $P(|\gamma_{i,s}| \leq \sigma|\tau) = 0.05$  and  $P(|\gamma_{i,s}| \leq \sigma|\tau) = 0.01$  corresponding to  $\tau = 1.92$  (—) and  $\tau = 3.32$  (- -), respectively.

This structure combines strong penalization of coefficients near zero with minimal shrinkage of large coefficients. For  $|\gamma_{j,s}| \gg 0$ , the exponential term becomes negligible and the density decays polynomially at rate  $|\gamma_{j,s}|^{-2}$  (see Johnson and Rossell, 2010), so that the induced bias on large break estimates is of order  $O(1/(T|\gamma_{j,s}|^3))$  (see Proposition 2 in Rossell and Telesca, 2017), which is negligible relative to the  $O_p(T^{-1/2})$  sampling variability of the least-squares estimator. Thinner-tailed slab priors, by contrast, may impose excessive shrinkage on large breaks, particularly in short samples.

The resulting specification is therefore coherent across all of the three desired properties: the Dirac spike sets excluded coefficients exactly to zero; the non-local slab ensures rapid discrimination against spurious breaks and delivers model selection consistency in the high-dimensional ISR setting; and the heavy tails of the iMOM density allow included breaks to be estimated without undue shrinkage toward the null.

It is well known that model selection using SSVS is sensitive to the choice of the slab scale parameter. Hierarchical specifications partially address this issue by introducing an additional hyperprior, which may increase computational complexity. In contrast, the scale parameter  $\tau$  of the iMOM prior has a natural and interpretable role, as it directly governs the prior probability that a break magnitude lies within a neighbourhood of zero, allowing explicit control over the prior mass, and thus shrinkage imposed on small breaks.

This interpretation facilitates calibration based on the prior probability  $P(|\gamma_j| \leq \bar{\gamma} | \tau)$  for a chosen threshold  $\bar{\gamma} > 0$ . For example, setting  $\bar{\gamma} = \sigma$  and choosing  $\tau = 1.92$  ( $\tau = 3.32$ ) implies that the prior probability of a break lying within  $(-\sigma, \sigma)$  is below 0.05 (0.01). Equivalently, this limits the prior probability of a break with signal-to-noise ratio  $|\gamma_j|/\sigma \leq 1$  to 0.05 and 0.01, respectively. Figure 1 illustrates the implied prior densities for these values of  $\tau$ .

Framing the break detection problem as a model selection exercise further allows for the use of posterior inclusion probabilities (PIPs) for each break to assess the evidence for its inclusion. Within this framework, PIPs provide a natural measure of uncertainty for individual break indicators. A common decision rule selects breaks with  $PIP > 0.5$ , corresponding to the median probability model (Barbieri and Berger, 2004). This threshold minimizes classification risk under standard loss functions and provides an intuitive criterion for break detection. More generally, aggregating PIPs across adjacent time

points yields a probabilistic measure of break timing, which is particularly useful when structural changes are gradual or weak but persistent.

In the absence of strong prior information on the proportion of structural breaks, the prior inclusion probability  $\omega_{i,s}$  may be specified uniformly,  $\omega_{i,s} = \omega$ . Alternatively,  $\omega_{i,s}$  can be treated as unknown and assigned a hyperprior, such as a Beta distribution (see, for example, Scott and Berger, 2010), allowing the sparsity level to be learned from the data. As with  $\tau$ , however, hierarchical specifications may affect mixing and convergence when the data are weakly informative.

#### 2.4. Outlier Robustness

The reliable detection of step-shifts may be compromised by outliers, as extreme observations can generate spurious break signals or distort estimated break magnitudes. To enhance robustness, the baseline model is extended by specifying a mixture distribution for the disturbance term  $\varepsilon_{i,t}$  and introducing a data augmentation step that probabilistically rescales observations during estimation.<sup>3</sup>

We assume the disturbance term follows the mixture distribution

$$p(\varepsilon_{i,t}) = (1 - \delta_{i,t}^\varepsilon) \pi_N(\varepsilon_{i,t}; 0, \sigma_i^2) + \delta_{i,t}^\varepsilon \pi_{iMOM}(\varepsilon_{i,t}; 0, 1, 3, \sigma^2 \tau^\varepsilon), \quad (2.8)$$

$$p(\delta_{i,t}^\varepsilon) = \eta^{\delta_{i,t}^\varepsilon} (1 - \eta)^{1 - \delta_{i,t}^\varepsilon}, \quad (2.9)$$

where  $\pi_N(\cdot; 0, \sigma_i^2)$  denotes the Gaussian density with mean zero and variance  $\sigma_i^2$ ,  $\delta_{i,t}^\varepsilon \in \{0, 1\}$  indicates whether observation  $(i, t)$  is classified as an outlier, and  $\eta \in (0, 1)$  is the prior inclusion probability. Note that we need  $\nu = 3$  here for the variance to exist. Under this specification, non-outlying observations follow the Gaussian distribution, while outliers are governed by the heavy-tailed iMOM distribution. Posterior inference on  $\delta_{i,t}^\varepsilon$  therefore provides a probabilistic classification of outliers.

To mitigate their influence, observations classified as outliers are downweighted in subsequent estimation steps by the inverse standard deviation of the iMOM distribution,  $1/\sqrt{2\tau^\varepsilon} \ll 1$ . Conditional on  $\delta_{i,t}^\varepsilon$  and  $\tau^\varepsilon$ , the rescaled residual at each Gibbs iteration is

$$\tilde{\varepsilon}_{i,t} = (1 - \delta_{i,t}^\varepsilon) \hat{\varepsilon}_{i,t} + \delta_{i,t}^\varepsilon \frac{\hat{\varepsilon}_{i,t}}{\sqrt{2\tau^\varepsilon}}, \quad (2.10)$$

where  $\hat{\varepsilon}_{i,t}$  denotes the model residual implied by equation (2.2). This rescaling attenuates the influence of extreme observations while preserving the information content of the remaining data.

The resulting specification induces a flexible error structure with observation-specific variance inflation driven by posterior outlier probabilities. Conceptually, this approach is related to Bayesian models with observation-specific volatility, such as stochastic volatility models (e.g., Jacquier et al., 2002; Kastner and Frühwirth-Schnatter, 2014), while remaining computationally tractable within the indicator-saturated regression framework.

<sup>3</sup>Frequentist approaches achieve robustness by introducing impulse indicators and selecting among them via impulse indicator saturation (Castle et al., 2015; Pretis and Schwarz, 2022), typically in a separate pre-estimation step. In contrast, our approach integrates outlier detection directly within the Bayesian estimation procedure.

### 3. IDENTIFYING STEP-SHIFTS: A SIMULATION STUDY

We evaluate the performance of BISAM using a simulation study in which we compare its break detection accuracy to two established approaches: the general-to-specific (GETS) testing procedure (Castle et al., 2015; Pretis and Schwarz, 2022) and the adaptive Least Absolute Shrinkage and Selection Operator (ALASSO) regularisation method (Tibshirani, 1996).

The simulation design reflects empirical settings commonly encountered in applied work on structural break detection for climate policy evaluation. Specifically, we consider a panel with ten cross-sectional units ( $N = 10$ ) and thirty time periods ( $T = 30$ ). Data are generated under the assumption of homoskedastic disturbances with variance  $\sigma^2 = 1$ , and the data-generating process includes both time and cross-sectional fixed effects. We simulate structural breaks of varying magnitude, with break sizes given by  $\gamma \in \{1, 1.5, 2, 3, 6, 10\}$ . For each break magnitude, we generate 100 independent datasets and use each of the competing models to identify step-shifts. This design allows us to assess the relative performance of BISAM and alternative methods across a range of signal strengths.

We consider two simulation environments that differ in the frequency of structural breaks: a sparse design and a dense design. In the sparse setting, four out of ten units exhibit exactly one break, occurring at a randomly selected time period. In the dense setting, eight out of ten units experience structural breaks, of which four units exhibit two breaks each.<sup>4</sup>

For the BISAM specification, we set the slab scale parameter to  $\tau \approx 3.32$ , which implies  $P(|\gamma| \leq \sigma | \tau) = 0.01$ . This calibration assigns 99% of the prior mass of the slab component to values outside one standard deviation of the disturbance term, thereby favouring a priori the detection of “sufficiently large” breaks. For the GETS procedure, we adopt a nominal significance level of  $\alpha = 0.01$ ,<sup>5</sup> reflecting standard practice in the structural break detection literature for the evaluation of climate policies. For the ALASSO estimator, we follow Zou (2006) and use a Ridge regression estimator in the first stage to construct adaptive weights, which are then employed in the penalised estimation step.

We evaluate performance using standard classification metrics. In particular, we compute:

- The true positive rate (*TPR*) and false positive rate (*FPR*), defined as the proportion of correctly detected breaks among true breaks and the proportion of falsely detected breaks among non-break candidates, respectively.
- *Precision*, defined as the proportion of correctly detected breaks among all detected breaks.
- The *F1 score*, defined as the harmonic mean of precision and TPR, and which provides a summary measure of detection accuracy.
- *Near misses*, defined as the proportion of undetected true breaks for which a break is incorrectly detected in an adjacent period, relative to the total number of missed breaks.

<sup>4</sup>Representative simulated datasets for the sparse and dense designs, together with their corresponding estimated PIPs, are presented in the Appendix.

<sup>5</sup>Under suitable assumptions, this nominal level can be related to a target false positive rate under the null hypothesis of no structural breaks (Pretis and Schwarz, 2022).

Figure 2 and Figure 3 present the results of the simulation study across break magnitudes for the sparse and dense break environments, respectively. In the sparse design, BISAM and GETS exhibit broadly comparable performance, and both substantially outperform ALASSO across all evaluation metrics. BISAM tends to be more conservative, exhibiting a slightly lower TPR but higher precision than GETS. As a result, both methods achieve similar F1 scores across most break magnitudes.

The results for the near miss metric partly exhibit an inverse-U-shaped pattern, with the proportion of near misses increasing for break magnitudes up to approximately three times the standard deviation of the disturbance term, and declining sharply thereafter. This pattern indicates that, for moderately sized breaks, both BISAM and GETS more frequently detect structural breaks in periods adjacent to the true break location. Even in cases where the TPR of BISAM and GETS remains relatively low to moderate (approximately 0.3 and 0.8, respectively), both methods capture signals in the vicinity of the true breakpoints.

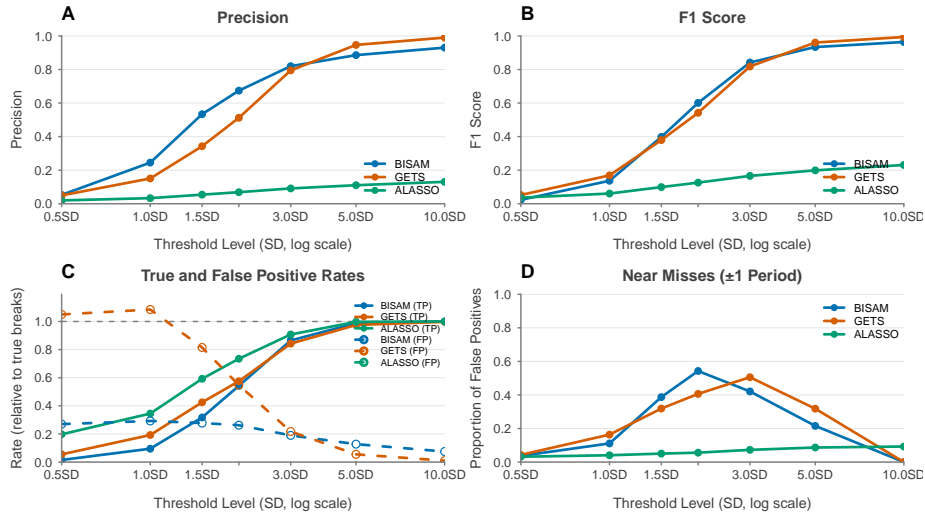


**Figure 2.** Performance metrics (BISAM, GETS, ALASSO) for the simulation setting with a sparse break environment, for varying relative break size (measured in standard deviations of the error term).

Differences across methods become more pronounced in environments with a higher frequency of structural breaks. In the dense break setting, GETS exhibits substantially weaker break detection performance. Even for large break magnitudes exceeding three standard deviations of the disturbance term, both precision and F1 scores decline markedly. This deterioration is primarily driven by a reduction in true positive rates, while false positive rates remain comparatively stable across break sizes. In contrast, BISAM maintains stable performance across break magnitudes and consistently outperforms both GETS and ALASSO in detection accuracy. Figure 4 further illustrates this pattern across varying numbers of breaks. While the performance of GETS deteriorates as the number of breaks increases, BISAM preserves high detection accuracy throughout.

The performance of ALASSO improves as the number of breaks increases. However,

this improvement largely reflects the mechanical effect of a shrinking set of non-break candidates, which reduces the scope for false positive classifications, rather than a systematic improvement in its ability to correctly identify true structural breaks.

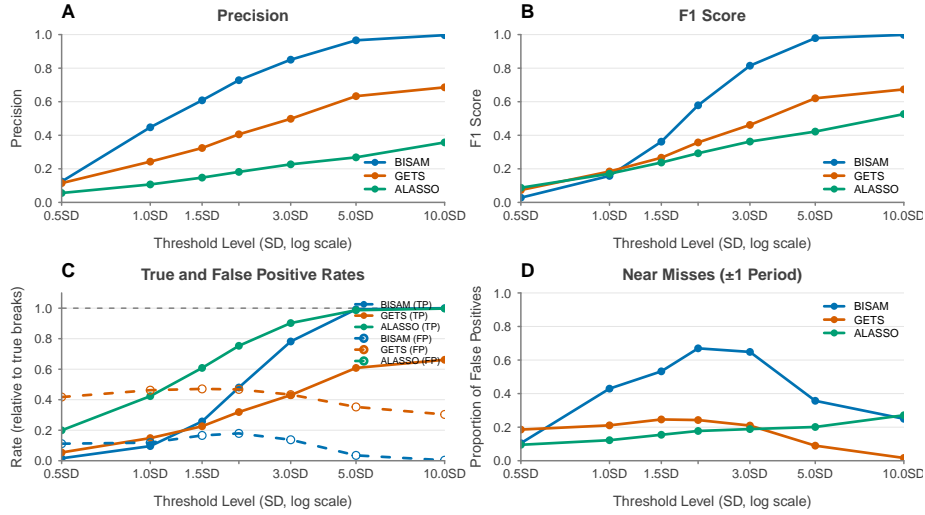


**Figure 3.** Performance metrics (BISAM, GETS, ALASSO) for the simulation setting with a dense break environment, for varying relative break size (measured in standard deviations of the error term).

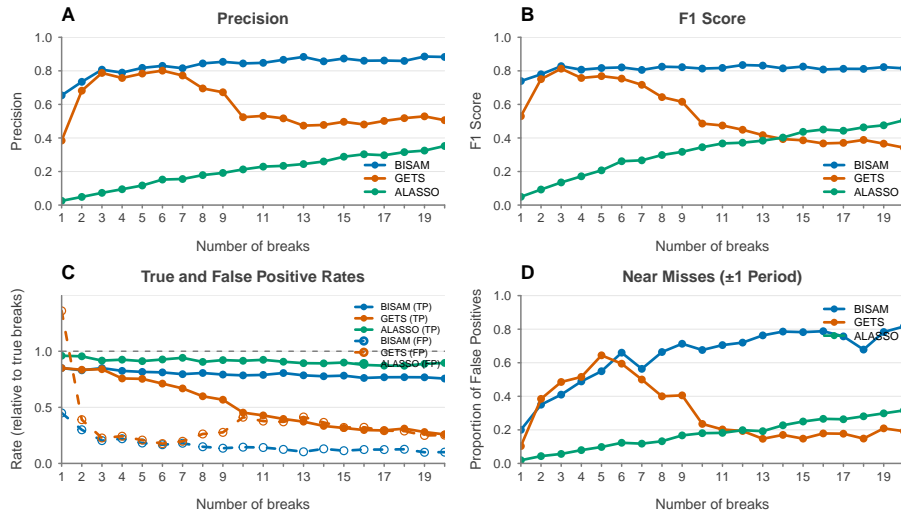


**Figure 4.** Performance metrics (BISAM, GETS, ALASSO) for simulations assuming a relative break size of three standard deviations of the error term ( $\sigma^2$ ) and varying number of breaks.

The simulation results demonstrate that BISAM provides a reliable and robust framework for structural break detection in high-dimensional panel settings. While BISAM and GETS perform similarly in sparse environments, BISAM exhibits substantially greater stability and accuracy as the number of breaks increases. In particular, BISAM maintains consistently high precision and F1 scores across break magnitudes and break frequencies, whereas the performance of GETS deteriorates markedly in settings with higher break density due to declining true positive rates. Compared to ALASSO, BISAM delivers superior detection accuracy across all designs, especially for moderate break magnitudes.

#### 4. HOW EFFECTIVE ARE CLIMATE CHANGE MITIGATION POLICIES IN THE TRANSPORT SECTOR? A REASSESSMENT

Having established the favourable finite-sample properties of BISAM in our controlled simulation setting, we turn to an empirical application to evaluate its performance as a tool for climate policy evaluation. For that purpose, we apply BISAM to study the effectiveness of climate policies in the European road transport sector. We assess the empirical application in Koch et al. (2022) and contrast our findings with those obtained using the GETS procedure.

The econometric analysis in Koch et al. (2022) seeks to identify structural breaks in greenhouse gas emissions from the transport sector across 15 European countries and, in a subsequent step, attribute negative breaks to the implementation of transport-related climate policies. To this end, the authors employ a step-shift indicator-saturated (SIS) specification analogous to equation (2.2), using log CO<sub>2</sub> emissions from the transport sector as the dependent variable and including log GDP (and its square) and population as control variables besides unit and time fixed effects.

The emissions data consist of annual observations covering the period 1995–2018 for 15 EU countries (Austria, Belgium, Germany, Denmark, Spain, Finland, France, United Kingdom, Ireland, Italy, Luxembourg, Netherlands, Greece, Portugal, and Sweden), and are obtained from the Emissions Database for Global Atmospheric Research (EDGAR) v5.0 (Crippa et al., 2019). Data on GDP and population are sourced from the World Bank Open Data.

In the absence of strong prior information about the magnitude of potential structural breaks in emissions, we set the slab scale parameter to  $\tau \approx 1.92$ . This calibration implies that 95% of the prior mass of the slab component is assigned to values outside one standard deviation of the (country-specific) disturbance term. For the GETS procedure, we adopt a nominal significance level of  $\alpha = 0.05$ , which is consistent with the specification used in Koch et al. (2022).

Figure 5 summarises the empirical results. In the upper panels, dashed vertical lines indicate breaks detected by BISAM using a posterior inclusion probability threshold of  $P(\gamma_{i,s} \neq 0 | y) \geq 0.5$  at individual dates, while crosses denote breaks identified by the GETS procedure. Shaded regions represent intervals of varying length ( $\bar{t}^{\{1,2,3\}}$ ) over which BISAM detects structural changes, with orange and green shading corresponding to negative and positive breaks, respectively. The lower panels display the observed transport sector emissions over the period 1995–2018, together with the fitted values implied by the BISAM specification.

Our empirical findings broadly corroborate the main conclusions in Koch et al. (2022), while also revealing systematic differences in break detection and policy attribution. Koch et al. (2022) identify ten statistically significant emission reductions across EU countries

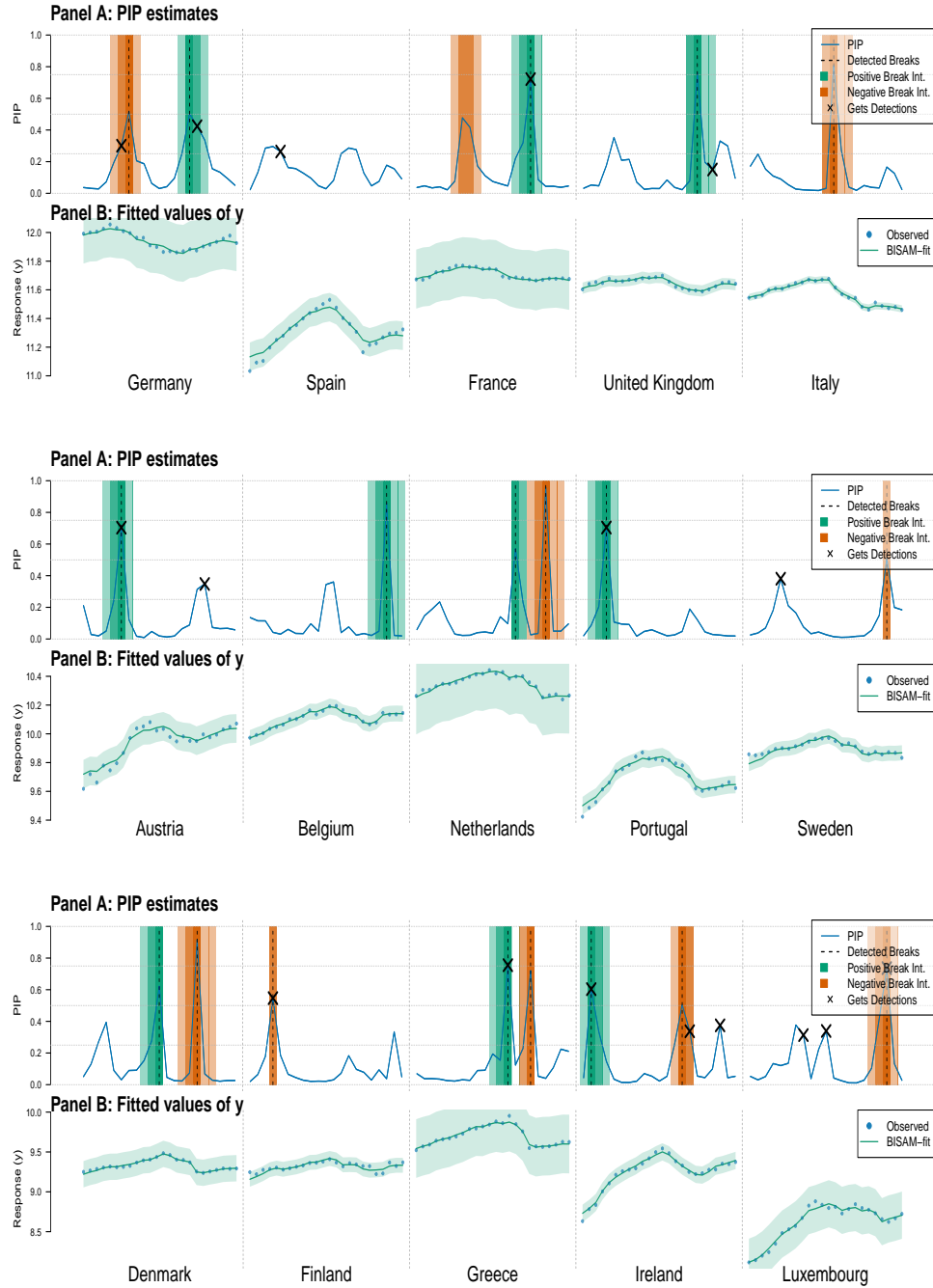


**Figure 5.** Break detection in EU transport emissions. Breaks detected by GETS (black crosses) and BISAM (vertical dashed lines). Green (orange) shaded areas indicate periods in which BISAM detects positive (negative) breaks. Transparency of shading corresponds to (inverse) interval length in which a break has been found for  $\bar{t}_{\{1,2,3\}}$ .

over the period 1995–2018, with estimated reductions ranging between 8% and 26%, and attribute these breaks primarily to policy mixes involving carbon or fuel taxation combined with vehicle-related incentives. Consistent with these findings, BISAM detects a substantial overlap in the timing and location of major structural breaks, especially those associated with large and persistent reductions in transport emissions. This result provides external validation of the structural break detection framework and confirms that the largest emission reductions coincide with major policy interventions affecting the marginal cost of transport-related emissions.

At the same time, BISAM uncovers additional negative structural breaks that are not detected by the GETS procedure. These breaks point to sustained emission declines in several countries, including France (2003–05), Italy (2007–10), the Netherlands (2012–16), Sweden (2015), Denmark (2010–14), and Greece (2010–13), where the years in parentheses denote the estimated break intervals. We follow Koch et al. (2022) and attribute these breaks to climate policies targeting the road transport sector. To identify relevant measures, we use the Policies Database of the International Energy Agency (IEA) and the IFCMA Climate Policy Database of the OECD.<sup>6</sup>

France (2003–05) implemented the *Plan Climat*, signed in 2004, which introduced measures to improve urban transport efficiency, promote lower-carbon transport modes, and establish biofuel targets that were subsequently enacted into law. Italy (2007–10) increased biofuel quotas in 2008 and introduced purchase incentives for cleaner vehicles between 2007 and 2009, alongside the *Milan Ecopass* congestion charge launched in January 2008.

The Netherlands (2012–16) introduced incentives for zero-emission vehicles and plug-in hybrids, together with a 2015 administrative agreement on zero-emission transport. Over the same period, the legally mandated share of renewable energy in transport fuels increased from about 4.5% in 2012 to 6.25% in 2015. Sweden (2015) did not implement a single major reform in that year, but continued increases in biofuel blending and the congestion tax introduced in Gothenburg in 2013 likely contributed with some delay.

Denmark (2010–14) increased the mandatory biofuel share in transport fuels from near zero to approximately 5.75%, supported by the *Sustainable Transport Plan* adopted in 2008, which included measures to improve transport efficiency, expand public transport, and promote cleaner transport technologies. Greece (2010–13) represents a case where economic and policy forces jointly contributed to emission reductions: fuel taxes were raised as part of austerity programs beginning in 2010, economic contraction reduced transport demand, and Law 3831/2010 reformed vehicle taxation and introduced provisions aimed at reducing air pollution.

## 5. CONCLUSIONS

In this study, we introduce Bayesian Indicator Saturated Modelling (BISAM), a probabilistic framework for detecting structural breaks in panel data. Our approach builds upon a linear regression specification saturated with step-shift indicators that exhaustively represent the full set of potential breakpoints. To select among these candidate breaks, we employ a spike-and-slab mixture prior combining a Dirac spike and a non-local (inverse-moment density) slab component. This probabilistic formulation enables

<sup>6</sup>These databases are available at <https://www.iea.org/policies> and <https://www.oecd.org/en/data/datasets/ifcma-climate-policy-database.html>.

coherent uncertainty quantification for individual breaks as well as combinations thereof, facilitating the detection of weaker signals that may persist over extended periods. The model also features an integrated treatment of outlier observations.

We demonstrate the accuracy and robustness of BISAM in simulation studies and benchmark its performance against established frequentist alternatives (GETS and adaptive LASSO). Standard performance metrics indicate that BISAM achieves superior detection accuracy while effectively controlling false positives, particularly in environments characterised by multiple structural breaks. Its detection performance remains stable as the number of breaks increases, making it especially well suited to applications in which the number and timing of structural changes are unknown and potentially large.

We illustrate the empirical relevance of BISAM for policy evaluation by revisiting the analysis of emission reductions in the European road transport sector by Koch et al. (2022). While BISAM largely confirms the timing of major emission reductions identified in the existing literature, it also uncovers additional negative structural breaks in countries such as France, Italy, the Netherlands, Sweden, Denmark, and Greece, indicating more persistent and gradual emission declines than previously detected. These additional breaks align closely with the timing of transport-related climate policies, including biofuel mandates, vehicle purchase incentives, and congestion pricing schemes. Taken together, these findings highlight the ability of BISAM to detect sustained structural changes associated with policy interventions and underscore its usefulness as a general and reliable tool for structural break detection in longitudinal settings.

#### ACKNOWLEDGEMENTS

The authors would like to thank Felix Pretis and Moritz Schwarz for helpful methodological discussions, Jakob Goldmann for assistance in improving the `bisam` package and David Rossell for support on tailoring the `mombf` to our needs. Support by the Vienna Science and Technology Fund under grant ESS22-040 is acknowledged.

#### CODE & DATA AVAILABILITY

All code and data to estimate Bayesian Indicator Saturated Models and replicate the findings presented in this paper are available at [https://github.com/konradld/EctJ\\_climate\\_policy\\_breaks](https://github.com/konradld/EctJ_climate_policy_breaks).

#### REFERENCES

- Barbieri, M. M. and J. O. Berger (2004). Optimal predictive model selection. *Annals of Statistics* 32(1), 870–897.
- Bayarri, M. J. and G. García-Donato (2007). Extending conventional priors for testing general hypotheses in linear models. *Biometrika* 94(1), 135–152.
- Carvalho, C. M., N. G. Polson, and J. G. Scott (2010). The horseshoe estimator for sparse signals. *Biometrika* 97(2), 465–480.
- Castle, J. L., J. A. Doornik, and D. F. Hendry (2012). Model selection when there are multiple breaks. *Journal of Econometrics* 169(2), 239–246.
- Castle, J. L., J. A. Doornik, D. F. Hendry, and F. Pretis (2015). Detecting Location Shifts during Model Selection by Step-Indicator Saturation. *Econometrics* 3(2), 240–264.
- Chipman, H. A., E. I. George, and R. E. McCulloch (2010). BART: Bayesian additive regression trees. *Annals of Applied Statistics* 4(1), 266–298.

- Crippa, M., G. Oreggioni, D. Guizzardi, M. Muntean, E. Schaaf, E. Lo Vullo, E. Solazzo, F. Monforti-Ferrario, J. G. Olivier, and E. Vignati (2019). Fossil co2 and ghg emissions of all world countries. *Publication Office of the European Union: Luxemburg*, 1–251.
- George, E. I. and R. E. McCulloch (1993). Variable selection via gibbs sampling. *Journal of the American Statistical Association* 88(423), 881–889.
- George, E. I. and R. E. McCulloch (1997). Approaches for Bayesian variable selection. *Statistica Sinica*, 339–373.
- Imbens, G. W. and J. M. Wooldridge (2009). Recent Developments in the Econometrics of Program Evaluation. *Journal of Economic Literature* 47(1), 5–86.
- Ishwaran, H. and J. S. Rao (2005). Spike and slab variable selection: Frequentist and Bayesian strategies. *Annals of Statistics* 33(2), 730–773.
- Jacquier, E., N. G. Polson, and P. E. Rossi (2002). Bayesian analysis of stochastic volatility models. *Journal of Business & Economic Statistics* 20(1), 69–87.
- Jeffreys, H. (1998). *The theory of probability* (Third edition ed.). Oxford University Press.
- Johnson, V. E. and D. Rossell (2010). On the use of non-local prior densities in bayesian hypothesis tests. *Journal of the Royal Statistical Society. Series B (Statistical Methodology)* 72(2), 143–170.
- Johnson, V. E. and D. Rossell (2012). Bayesian model selection in high-dimensional settings. *Journal of the American Statistical Association* 107(498), 649–660.
- Kastner, G. and S. Frühwirth-Schnatter (2014). Ancillarity-sufficiency interweaving strategy (ASIS) for boosting MCMC estimation of stochastic volatility models. *Computational Statistics & Data Analysis* 76, 408–423.
- Koch, N., L. Naumann, F. Pretis, N. Ritter, and M. Schwarz (2022). Attributing agnostically detected large reductions in road CO2 emissions to policy mixes. *Nature Energy* 7, 844–853.
- Li, D., J. Qian, and L. Su (2016). Panel data models with interactive fixed effects and multiple structural breaks. *Journal of the American Statistical Association* 111(516), 1804–1819.
- Mitchell, T. J. and J. J. Beauchamp (1988). Bayesian variable selection in linear regression. *Journal of the american statistical association* 83(404), 1023–1032.
- O’Hagan, A. (1995). Fractional Bayes Factors for Model Comparison. *Journal of the Royal Statistical Society: Series B (Methodological)* 57(1), 99–118.
- Pretis, F. (2022). Does a Carbon Tax Reduce CO2 Emissions? Evidence from British Columbia. *Environmental and Resource Economics* 83(1), 115–144.
- Pretis, F. and M. Schwarz (2022). Discovering What Mattered: Answering Reverse Causal Questions by Detecting Unknown Treatment Assignment and Timing as Breaks in Panel Models.
- Qian, J. and L. Su (2016). Shrinkage estimation of common breaks in panel data models via adaptive group fused Lasso. *Journal of Econometrics* 191(1), 86–109.
- Rossell, D. and D. Telesca (2017). Nonlocal priors for high-dimensional estimation. *Journal of the American Statistical Association* 112(517), 254–265.
- Santos, C., D. F. Hendry, and S. Johansen (2008). Automatic selection of indicators in a fully saturated regression. *Computational Statistics* 23, 317–335.
- Scott, J. G. and J. O. Berger (2010). Bayes and empirical-bayes multiplicity adjustment in the variable-selection problem. *The Annals of Statistics*, 2587–2619.
- Stechemesser, A., N. Koch, E. Mark, E. Dilger, P. Klösel, L. Menicacci, D. Nachtigall, F. Pretis, N. Ritter, M. Schwarz, et al. (2024). Climate policies that achieved major emission reductions: Global evidence from two decades. *Science* 385(6711), 884–892.

- Tebecis, T. and J. Crespo Cuaresma (2025). A dataset of structural breaks in greenhouse gas emissions for climate policy evaluation. *Scientific Data* 12(1), 42.
- Tibshirani, R. (1996). Regression shrinkage and selection via the Lasso. *Journal of the Royal Statistical Society B* 58(1), 267–288.
- Zellner, A. (1986). Bayesian estimation and prediction using asymmetric loss functions. *Journal of the American Statistical Association* 81(394), 446–451.
- Zou, H. (2006). The adaptive lasso and its oracle properties. *Journal of the American Statistical Association* 101(476), 1418–1429.

APPENDIX: SELECTED SIMULATION RESULTS

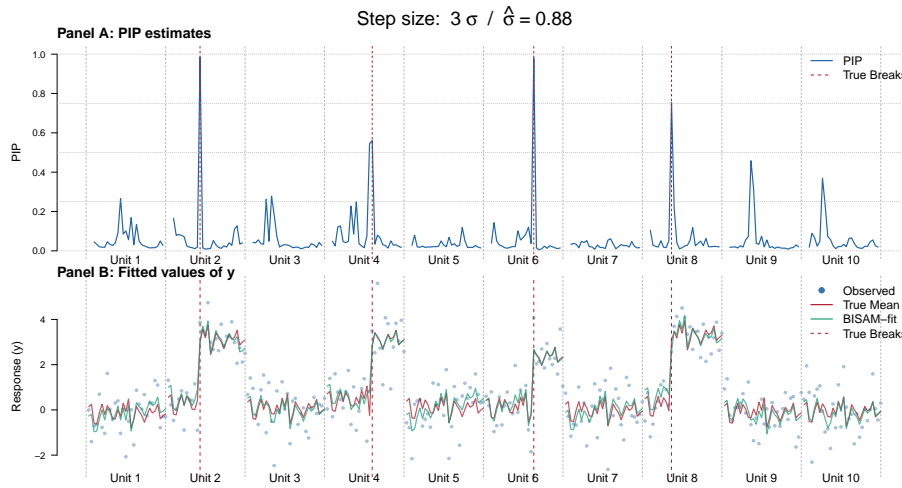


**Figure A.1.** Sparse simulation setup. Posterior inclusion probabilities in the upper panel. Lower panel shows the simulated data points (blue dots), the true mean (red line) and the fit of BISAM. Red dashed lines indicate true breaks.

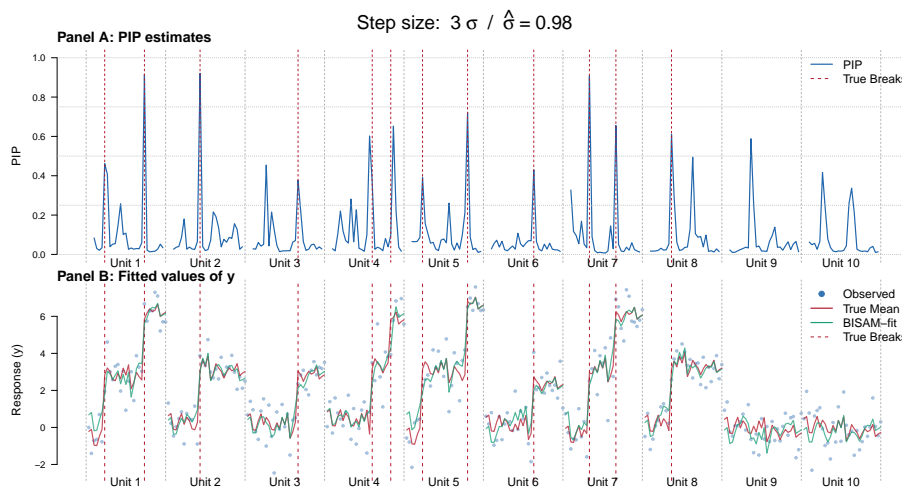


**Figure A.2.** Dense simulation setup. Posterior inclusion probabilities in the upper panel. Lower panel shows the simulated data points (blue dots), the true mean (red line) and the fit of BISAM. Red dashed lines indicate true breaks.